PHYSICAL REVIEW E

STATISTICAL PHYSICS, PLASMAS, FLUIDS, AND RELATED INTERDISCIPLINARY TOPICS

THIRD SERIES, VOLUME 60, NUMBER 2 PART B AUGUST 1999

ARTICLES

Simulations of fluid hydrogen: Comparison of a dissociation model with tight-binding molecular dynamics

Thomas J. Lenosky,* Joel D. Kress, and Lee A. Collins
Theoretical Division, Los Alamos National Laboratory, Los Alamos, New Mexico 87545

Ronald Redmer and Hauke Juranek
Fachbereich Physik, Universität Rostock, D-18051 Rostock, Germany

(Received 19 February 1999)

We compare the results of two complementary approaches, tight-binding molecular-dynamics simulations and a dissociation model, for determining the characteristics of dense, fluid hydrogen at pressures extending to megabars and temperatures to 10 000 K. Two tight-binding models were examined: one parametrization emphasized crystalline, molecular, and fluid properties, the other focused more on the intricate molecular interactions involving up to four hydrogen atoms. The two tight-binding cases and the dissociation model agree reasonably well for a variety of properties, including the equation of state, dissociation degree, and proton pair-correlation functions. In simulations of recently reported laser-driven shock experiments, the tight-binding and dissociative models predict different maximum compressions of four and five, respectively. We discuss the sensitivities of the models as well as give estimates for the region of validity of the chemical picture (dissociation model) and the accuracy of the dynamical picture (tight-binding simulations) in cases where molecular hydrogen still dominates the physical behavior. [S1063-651X(99)02608-2]

PACS number(s): 05.70.Ce, 52.25.Kn, 62.90.+k, 64.30.+t

I. INTRODUCTION

The behavior of fluid hydrogen derived from recent shock-wave experiments shows distinct features at Mbar pressures and finite temperatures. While metallization of solid hydrogen near $T=0$ K has not been verified up to 3 Mbar so far, metalliclike conductivities have been observed in shock-compression experiments using a two-stage light gas gun in the fluid domain around 1.4 Mbar and 3000 K [1]. Furthermore, significant discrepancies between the Hugoniot curves derived from laser-driven shock-wave experiments [2,3] and those using rather simplified theoretical equations of state such as the Sesame tables [4] have been found in the Mbar region where fluid hydrogen seems to be much more compressible than predicted. Both effects would drastically change our present understanding of the behavior of matter at ultrahigh pressures relevant for models of planetary and stellar interiors and inertial confinement fusion studies.

New quantum statistical studies of hydrogen as the simplest Coulomb system have been stimulated by these experiments. We apply both a chemical and dynamical picture for the description of dense hydrogen at ultrahigh pressures in the Mbar region. In a chemical picture, composite particles such as atoms and molecules are taken as the elements of a statistical description of the system [5]. Starting with the neutral molecular fluid at low densities and not too high temperatures, the consideration of pressure dissociation extends the applicability of this method into the region of Mbar pressures and elevated temperatures up to about 10 000 K. The physical properties are derived from the effective interactions between these particles, which already reflect the many-particle nature of the system. The variation of the effective interactions and of the atomic and molecular properties with the density and temperature is the central problem within a chemical picture.

For the dynamical picture, a spatially replicated sample of particles move according to forces generated from model interaction potentials. These models cover a wide range of sophistication from simple pair potentials to elaborate quantum-mechanical descriptions. Simulation methods such

*Present address: Lawrence Livermore National Laboratory, Livermore, CA 94551.

as path-integral Monte Carlo (PIMC) [6], wave-packet molecular-dynamics (WPMD) [7], and quantum molecular-dynamics [both density-functional (DF) [8,9] and tight-binding (TB) [10] approaches], have been developed, which are capable of treating the quantum effects at various levels of rigor. For practical evaluations, however, simplifying assumptions are usually necessary. In the WPMD, antisymmetrization is limited to pairwise exchange while assumptions about the nodes of the density matrix must be made in the PIMC method. For the tight-binding molecular-dynamics (TBMD) case, the matrix elements of the interaction Hamiltonian take a prescribed functional form determined from a fit to accurate experimental and *ab initio* results. Furthermore, the limited computer capacity restricts an evaluation to finite samples of particles.

The dissociation model [11,12] has already been used to study the accuracy of WPMD simulations for the neutral fluid domain [13]. Reasonable agreement with the WPMD has been found for the proton-proton pair distribution function (PDF) at $r_s=2$ and $T=2000$ K and $T=5000$ K. We extend this study by comparing with dynamical models based on the TB and density-functional approaches for fluid hydrogen at temperatures of 2×10^3 K to 1×10^4 K and representative hydrogen mass densities of $\varrho=0.3344$ g/cm^3, 0.5257 g/cm^3, and 0.6177 g/cm^3. These parameters correspond to r_s values of 2.0, 1.72, and 1.63, respectively, where $r_s=d/a_B$ is the mean distance d between the electrons in units of the Bohr radius a_B. In this region, the transition from molecular, insulating hydrogen fluid to a state with metalliclike conductivities has been verified in shock-wave experiments [1].

The determination of the molecular dissociation degree as a function of the density and the calculation of the equation of state (EOS) is of central importance. The behavior of atomic states created by pressure dissociation in a dense, molecular medium remains an open problem, in particular, as to whether these electronic states are still localized or extended. A solution to this problem would give more insight into the mechanism of the nonmetal-to-metal transition observed. The proton-proton PDF $g_{\rm pp}(r)$, which gives the probability to find two protons at a distance r and, thus, structural information, is also determined within the two methods. We compare the analytical approach and the simulation method to extract regions where these models are applicable.

II. FORMULATIONS

A. Tight-binding molecular dynamics method

The total TB energy has the form [10]

$$E=\sum_i f_i\epsilon_i+\sum_{i<j} V(R_{ij}), \tag{1}$$

where f_i is the occupation number based on a Fermi–Dirac distribution at temperature T, V is an effective pair potential, and R_{ij} is the distance between atoms i and j. The eigenenergy ϵ_i comes from a solution of a generalized eigenvalue equation of the form

$$H\psi_i=\epsilon_i S\psi_i, \tag{2}$$

where H and S are the Hamiltonian and overlap matrices, respectively. Only a single s-type orbital occupies each atomic center. We performed nonlinear least-squares fits to find the optimal form of the functions $V(r)$, $h_{ss\sigma}(r)$, and $s_{ss\sigma}(r)$, which represent the pair potential, the two-center matrix elements of the Hamiltonian, and overlap matrices, respectively, that best reproduce a set of *ab-initio* and experimental results. The total internal energy per atom, U/N, then has the form

$$U/N=E/N+\frac{3}{2}k_BT_{\rm ion}, \tag{3}$$

where $T_{\rm ion}$ is the ion kinetic temperature and k_B is the Boltzmann constant.

We have developed two complementary TB models that emphasize different regimes. The original model, designated TB-I, has received extensive explication elsewhere [10]. TB-I was parametrized over a large span of information, including the diatomic molecule, various crystalline symmetries, and the fluid, to yield a model applicable over a broad range of density and temperature. On the other hand, we designed TB-II with greater emphasis on the low-temperature regime and, therefore, included more of the H_2 and H_4 characteristics as well as diamond anvil cell (DAC) data. Both models provide an effective representation of the direct Coulombic interactions, as well as the purely quantal mechanisms of exchange and correlation, and reasonably describe processes such as breaking and forming molecular bonds (dissociation $\leftrightarrow$ association), promoting and demoting electrons between states (excitation $\leftrightarrow$ de-excitation), and removing and binding electrons (ionization $\leftrightarrow$ recombination) as well as the basic motion of the nuclei.

The *ab initio* information used in constructing TB-II included (i) the ground and antibonding electronic states of H_2 as a function of internuclear separation [14], (ii) the $H+H_2$ reaction barrier, and (iii) the H_4 ground-state potential energy surface for 83 different atomic configurations [15]. In addition, we employed the DAC pressure data [16] at five points ($r_s=1.6$, 1.72, 1.85, 2.0, and 2.2). To gauge the predictive capabilities of the model, we determined other well-known molecular properties not included in the fit. For example, TB-II yields good structural properties for the crystalline states of hydrogen. Owing to the restrictive nature of the orbital basis, such models always necessitate compromise in the quality of fits to the various parameters. For TB-II, we sacrificed a small shift in the H_2 bond length ($1.4a_B$ to $1.38a_B$) to accommodate an accurate representation of the entire H_4 energy surface.

For each TB model, we performed constant-volume molecular-dynamics simulations with the Verlet algorithm within an isokinetic ensemble, maintained through velocity scaling. At each time step, we solve Eq. (2) for the eigenvalues and eigenvectors from which we generate the forces on each atom by Hellmann–Feynman prescriptions. The nuclei then move according to the classical equations of motion, based on these quantum-mechanically derived forces. Thus, the electrons receive a quantal treatment while the nuclei, a classical one. Local thermodynamical equilibrium was assumed whereby the electronic temperature in the Fermi–Dirac distribution was set to that of the ion motion (T

$=T_{\mathrm{ion}}$). Electronic states were computed at only the Γ point in reciprocal space. These aspects of the calculation were identical to Refs. [10]. We used a short time step of 0.2 fs, and a cubic periodic cell, typically with 250 atoms, in each case allowing the hydrogen to reach full equilibrium before collecting statistics for 3000–4000 time steps. Both static and dynamic properties appear well converged within better than a few percent as a function of the length of the simulations and the size of the samples. Properties determined from our standard 250-atom sample evince convergence to within a few percent compared to larger cases of 512 and 1024 atoms.

We determined the dissociation degree, or more precisely the fraction of monomers, by examining the nearest neighbor of each atom in the molecular-dynamics (MD) reference cell at a particular time step [10]. If two atoms form the nearest neighbor of each other, then they comprise a designated ''molecule.'' This analysis ranges over all the particles in the reference cell; atoms not associated with molecules are labeled monomers. The ratio of monomers to the total number of atoms gives the fraction of dissociation. The average of this fraction over time provides the reported measure of dissociation β. The scheme does not require the input of a specific bond length, as in many cluster analysis prescriptions. On the other hand, the formulation only allows monomers and dimers. Therefore, the scheme breaks down at higher densities where clusters containing many atoms may skew the results.

Finally, we have benchmarked the TB models by MD simulations within a finite-temperature density-functional (FTDF) approach. Both the local-density approximation (LDA) [8,9] and the generalized-gradient approximation (GGA) were employed at a select set of temperatures and densities. The GGA calculations were performed using the *ab-initio* total-energy and molecular dynamics program VASP (Vienna Ab-Initio Simulation Program) [17]. These simulations used very large plane-wave bases ($\sim 50\,000$) that effectively represented the excited and continuum states. These sophisticated FTDF methods allow us to gauge the accuracy of various approximations introduced into the TB models, for example, the use of a single *s*-type orbital on each atomic site. We should emphasize though that this constraint does not limit the TB models to the ground state of the H system since different linear combinations of these single atomic orbitals can form excited and ionized states of the whole system. For example, with two 1*s* orbitals on each H atom, we can represent both the ground ($^1\Sigma_g$) and first excited ($^1\Sigma_u$) states of H_2.

B. Dissociation model

In a chemical picture, hydrogen fluid is considered as a mixture consisting of H_2 molecules and H atoms interacting via effective potentials. At very high densities, modifications of the constituents and their interactions have to be treated in a systematic way. We will restrict our considerations to the region where these medium modifications are small. Furthermore, we consider low temperatures so that thermal ionization can be neglected. A corresponding dissociation model (DM) has been derived [11,12], which shows that pressure dissociation becomes important already in the shock-compressed, neutral fluid.

The composition of the system is given by the chemical equilibrium $\mu_{\mathrm{H}_2}=2\mu_{\mathrm{H}}$ for the reaction $\mathrm{H}_2 \rightleftharpoons \mathrm{H}+\mathrm{H}$. Usually, the chemical potentials are split into ideal and correlation contributions, i.e., $\mu_c=\mu_c^{\mathrm{id}}+\mu_c^{\mathrm{cor}}$ ($c=\mathrm{H},\ \mathrm{H}_2$). The dissociation degree β is defined by the partial densities in the fluid, $\beta=n_{\mathrm{H}}/(n_{\mathrm{H}}+2n_{\mathrm{H}_2})$. The molecules and atoms interact via effective two-body potentials, which approximate the effects of the real many-body interactions. Exponential-six potentials were taken to model the effective two-body interactions between the constituents; the parameters can be found elsewhere [11–13].

The fraction β of dissociated molecules is determined by the correlation contributions to the chemical potential according to

$$n_{\mathrm{H}_2}=\frac{n_{\mathrm{H}}^2\Lambda_{\mathrm{H}}^3}{\sqrt{2}}\sigma^{\mathrm{int}}\exp[(D_0-\mu_{\mathrm{H}_2}^{\mathrm{cor}}+2\mu_{\mathrm{H}}^{\mathrm{cor}})/k_BT],$$
$$\sigma^{\mathrm{int}}=\frac{k_BT}{hcB}\left[1-\exp\left(-\frac{hc\omega}{k_BT}\right)\right]^{-1}. \tag{4}$$

$D_0=4.735$ eV is the dissociation energy of isolated H_2 molecules and $\Lambda_{\mathrm{H}}^2=2\pi\hbar^2/(m_{\mathrm{H}}k_BT)$ the thermal wavelength of H atoms. σ^{int} denotes the internal partition function of vibrational and rotational states with $B=60.853\ \mathrm{cm}^{-1}$ and $\omega=4401\ \mathrm{cm}^{-1}$ as the characteristic rotational and vibrational constants of the H_2 molecule [18]; c is the speed of light.

We have calculated the correlation parts of the chemical potentials via $\mu_c^{\mathrm{cor}}=(\partial F_c^{\mathrm{cor}}/\partial N_c)_T$. The free energies for the pure molecular and atomic system are derived from fluid variational theory [19] using the effective pair potentials. The results for the EOS of the pure molecular (and atomic) subsystems agree with those obtained from classical Monte Carlo (MC) simulations up to Mbar pressures. The correlation contributions in Eq. (4) yield a lowering of the dissociation energy D_0 so that pressure dissociation becomes operative already in the neutral fluid. Neglecting these terms, almost no dissociation would occur at these conditions.

Three PDFs, $g_{\mathrm{H_2H_2}}$, $g_{\mathrm{H_2H}}$, and g_{HH}, are derived from classical MC simulations for the mixture of hydrogen molecules and atoms using again the effective pair potentials, the dissociation degree β, the temperature T, and the mass density ϱ as input. In order to extract the proton-proton PDF g_{pp} from these data, we need to determine the proton distribution in the H_2 molecule, which is very well known for isolated molecules in the singlet state [20]. Neglecting in-medium corrections to the molecular structure in Eq. (4) such as the vibron-shift [21,22] or a variation of the binding length of $1.4a_B$, the vibrational and rotational spectrum of the H_2 molecule can be derived by standard techniques. The probability of finding a proton at a distance r from another proton in the H_2 molecule at a temperature T is given by the eigenfunctions ϕ_i and eigenvalues E_i for the singlet potential via

$$w_{\mathrm{pp}}^{\mathrm{H_2}}(\mathbf{r})=\frac{\sum_i |\phi_i(\mathbf{r})|^2\exp(-E_i/k_BT)}{\sum_i \exp(-E_i/k_BT)}. \tag{5}$$

TABLE I. Pressures P, internal energies U, and dissociation degrees β based on the dissociation model (DM) given in Refs. [11,12] compared with those derived from the TBMD simulations of Ref. [10] (TB-I) and the present version (TB-II). Pressure in units of GPa, internal energy in eV/atom, and β in percent. Mass densities are for hydrogen.

		0.3344 g/cm^3 ($r_s=2$)			0.5257 g/cm^3 ($r_s=1.72$)			0.6177 g/cm^3 ($r_s=1.63$)		
Model	T (K)	P	U	β	P	U	β	P	U	β
DM	2000	21.6	−1.803	0.01	66.4	−1.417	1.73	91.6	−1.128	8.6
TB-I		22.0	−1.840	0.50	65.9	−1.451	2.0	90.0	−1.212	7.0
TB-II		19.1	−2.025	0.0	65.2	−1.690	0.1	97.3	−1.512	0.1
DM	3000	24.2	−1.616	0.44	67.0	−1.162	6.65	90.7	−0.874	14.6
TB-I		24.1	−1.622	2.0	65.1	−1.188	12.0	91.6	−0.978	16.0
TB-II		23.2	−1.782	0.10	71.3	−1.506	0.30	103	−1.284	0.80
DM	5000	28.1	−1.164	5.92	68.9	−0.654	17.3	92.5	−0.397	24.3
TB-I		26.7	−1.094	17.0	71.2	−0.764	27.0	102	−0.592	30.0
TB-II		28.5	−1.372	3.4	76.2	−0.970	8.4	109	−0.758	11.5
DM	7500	32.4	−0.531	17.6	74.1	−0.073	28.0	99.1	0.143	33.2
TB-I		32.7	−0.575	27.0	83.7	−0.320	32.0	119	−0.167	33.5
TB-II		34.3	−0.699	17.5	84.7	−0.384	22.9	120	−0.169	25.2
DM	10000	37.5	0.065	28.4	81.5	0.451	35.8	108	0.638	39.6
TB-I		40.9	−0.091	32.0	97.8	0.112	35.0	136	0.266	38.2
TB-II		42.0	−0.098	21.4	97.2	0.125	24.0	136	0.297	25.1

The ground and first-excited state were taken into account for the evaluation of Eq. (5), which is sufficient for the low temperatures considered here.

Recalling that the total number of protons is given by $n_p = n_H + 2n_{H_2}$, the proton-proton PDF is given by

$$g_{pp}(\mathbf{r}) = \frac{2n_{H_2}}{n_p^2} w_{pp}^{H_2}(\mathbf{r}) + \frac{n_H^2}{n_p^2} g_{HH}(\mathbf{r}) + \frac{4n_H n_{H_2}}{n_p^2} \int d^3s\, w_{pp}^{H_2}(\mathbf{s}) g_{HH_2}(\mathbf{r}-\mathbf{s}/2) + \frac{4n_{H_2}^2}{n_p^2} \int d^3s_1 \int d^3s_2 w_{pp}^{H_2}(\mathbf{s}_1) w_{pp}^{H_2}(\mathbf{s}_2) \times g_{H_2H_2}(\mathbf{r}-\mathbf{s}_1/2-\mathbf{s}_2/2). \quad (6)$$

The first term describes the internal proton-proton distribution in the H_2 molecule and the second one describes the proton-proton distribution for the H-H interaction. The third term represents the H-H_2 distribution, and the fourth one represents the H_2-H_2 contribution.

III. RESULTS

Before comparing the DM and TB models, we briefly discuss the results for the two TB cases in relation to the more sophisticated FTDF molecular-dynamics simulations. For the temperature and density range considered here, the GGA and TB-I remain in very good agreement both for static and dynamical properties. Diffusion coefficients, dissociation degree, internal energies, and pair-correlation functions show differences of 10% or less; only the pressure varies by as much as 20% at the higher densities and temperatures. The TB-II model departs from TB-I mainly in the degree of dissociation, as seen in Table I, with the former exhibiting less relative dissociation as the medium heats and compresses. Nevertheless, the region in which both models progress from a molecular to atomic fluid covers a very narrow ϱ–T space. If TB-I and TB-II start from the initial conditions of the laser experiments [2], namely, a molecular liquid at cryogenic temperatures, the respective Hugoniots lie very close, both yielding only a factor of four in compression. This should engender no surprise, as the TB models readily dissociate and rapidly move toward an atomic fluid at higher densities and temperatures.

Representative results for EOS properties (pressure P, internal energy U/N) and a descriptive property (the dissociation degree β) appear in Table I. The DM and TBMD show consistently similar trends across the whole span of study with noticeable disagreements beginning only at the highest densities and temperatures. This extreme probably marks the limits in both models since the fits for the TB cases did not extend much beyond $r_s=1.5$ and no ionization channels appear in this version of the DM.

We now examine in more detail the results in Table I and begin with the internal energy (U/N) by featuring a typical example in Fig. 1 for $r_s=2$ or a hydrogen mass density of

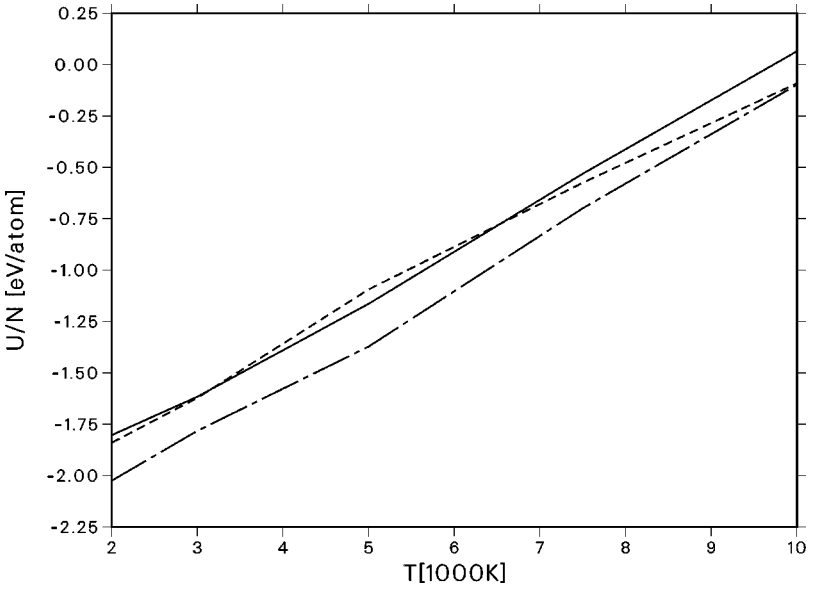

FIG. 1. Internal energy as a function of the temperature at $r_s=2$ for the DM (solid line), TB-I (dashed line), and TB-II (chain-dashed line) models.

$\rho=0.3344$ g/cm^3. We emphasize that all mass densities given in this paper, unless specifically noted as in the case of the Hugoniots, refer to hydrogen ($A=1$). At a fixed density, TB-II and DM parallel each other over the span of temperatures with the TB-II having the more negative value. TB-I remains closer to the DM model at lower temperatures, and to the TB-II model at higher temperatures. We observe similar trends at the other two densities. However, as the density increases, this crossover point moves to lower temperatures. The internal energy in all cases rises monotonically with temperature; no dramatic or abrupt changes occur. To view this in greater detail, we present in Fig. 2 for $r_s=1.63$ only the electronic component of the internal energy (E/N) with the ion kinetic contribution removed. A slight hysteresis exists in both the TB models that correlates closely with the regime of molecular dissociation. Pfaffenzeller and Hohl [23] observed similar behavior in DF-MD simulations of hydrogen at higher densities. Although a small inflection exists, this does not translate to the Hugoniot in any noticeable way. The internal energy appears well-behaved through this regime in density and temperature.

We observe more variation among the models for the dissociation degree β although only over the very narrow region from onset to the beginning of saturation in dissociation. As indicated in Fig. 3 for $r_s=1.72$, the TB models bracket the DM, indicating upper and lower limits of the number of monomers. Again, this is expected given that the TB-I and TB-II were constructed to highlight different aspects of this regime. At the higher density, TB-I and the DM agree best over the temperature range. Although the techniques for evaluating β in the two approaches differ, the dissociation preserves a common, general trend in this range.

To investigate the models further, we turn to the proton-proton PDF as derived from the DM and the TBMD simulations and present a representative example for $r_s=2$ and $T=5000$ K in Fig. 4. We compare not only the DM and TBMD cases but also the FTDF-GGA, WPMD, and PIMC. The DM, WPMD, and TB-II agree well while the PIMC shows a somewhat higher first peak, and the TB-I shows a somewhat lower first peak. The FTDF-GGA nearly coincides with the TB-I result.

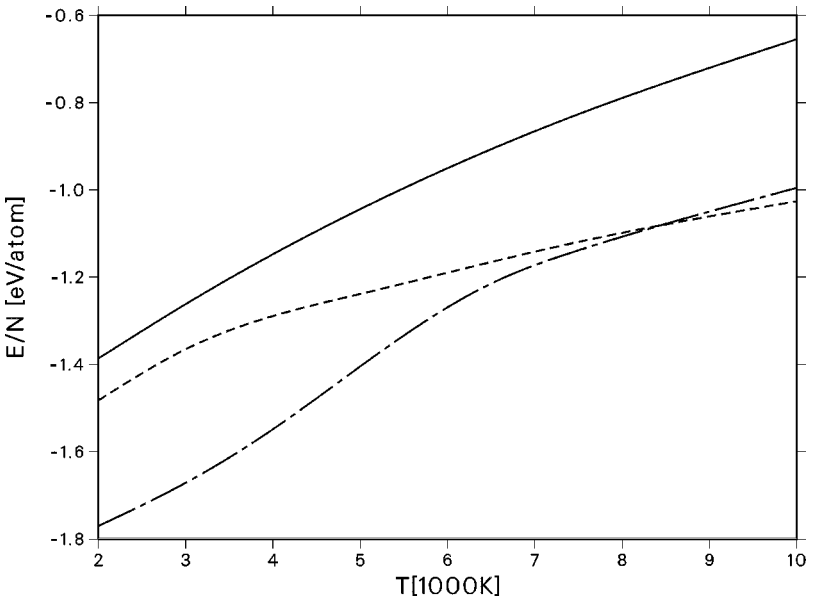

FIG. 2. Electronic component of the internal energy as a function of the temperature at $r_s=1.63$ for the DM (solid line), TB-I (dashed line), and TB-II (chain-dashed) models.

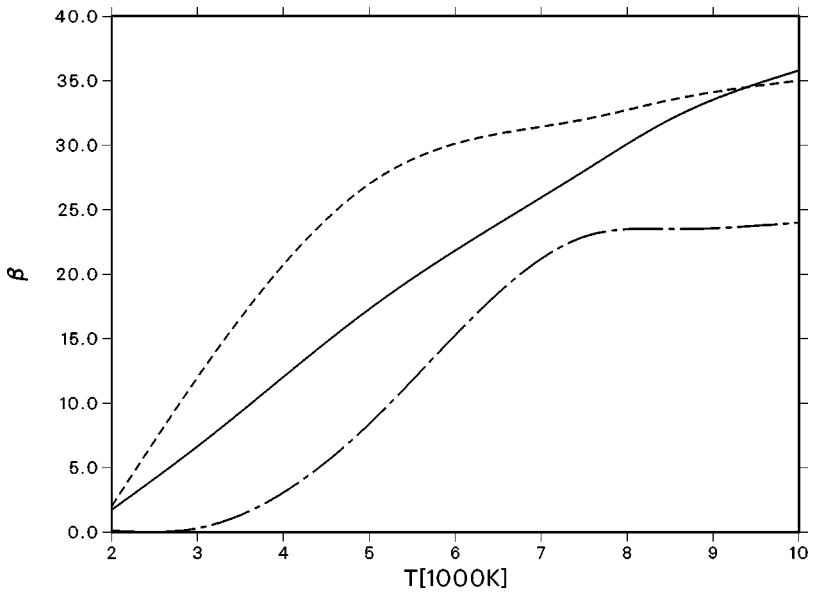

FIG. 3. Dissociation degree β as a function of the temperature at $r_s=1.72$ for the DM (solid line), TB-I (dashed line), and TB-II (chain-dashed line) models.

We explore the effects of density and temperature changes in Figs. 5–7 for the three densities ($r_s=2.0$, 1.72, and 1.63) and temperatures between 2000 K and 10 000 K. The general behavior is very systematic. The first peak occurs at the molecular bond length of $1.4a_B$ and is very pronounced at low temperatures indicating the molecular structure of hydrogen under these conditions. The first and second peaks become less pronounced as temperature and density rise due to an increasing fraction of dissociated molecules. Compressed hydrogen becomes less structured, and the atoms are located between the molecules. For higher densities, the differences become more pronounced as expected. Especially, the PDFs obtained from the TBMD simulations show significantly less structure than the DM for the highest temperatures; the first peak height is even smaller than the second one. The slight displacement in the first peak between the two approaches reflects the different values employed for the H_2 equilibrium distance, $1.4a_B$ in the DM and $1.38a_B$ in TB-II.

A seeming contradiction appears from a comparison of the average dissociation degree and the relative heights of the first (H_2) peak in the PDFs. For the β parameter, the DM and TB-I agree remarkably well over the entire range of densities and temperatures studied. Yet, at the higher temperatures, the heights of the molecular peak in their respective PDFs show considerable differences. An initial tendency arises to associate the peak height directly with β; however, this can result in misleading conclusions. Part of the problem rests with the procedures employed to define β. As indicated above, these yield at best semiquantitative results since they require certain definitions of a ''molecule,'' based on nearest-neighbor or bond-length constraints that do not universally apply in a transient, disordered system. A more reliable comparison involves integrating the PDF in the radial variable until the coordination number yields unity. This

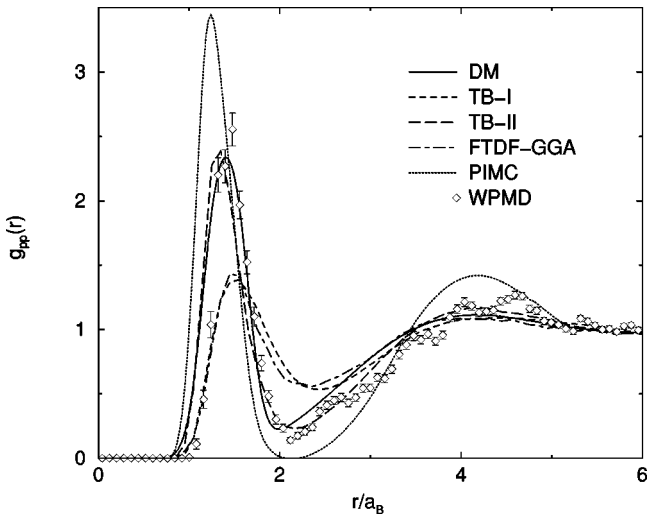

FIG. 4. Proton-proton pair distribution function for $r_s=2$ ($\varrho=0.3344$ g/cm^3) and $T=5000$ K: DM (solid line), TB-I (dashed line), TB-II (long-dashed line), and FTDF-GGA (dot-dashed line). The PIMC results of Magro and co-workers [6] (dotted line) and the PDF of the WPMD method (symbols, see [13]) are shown for comparison.

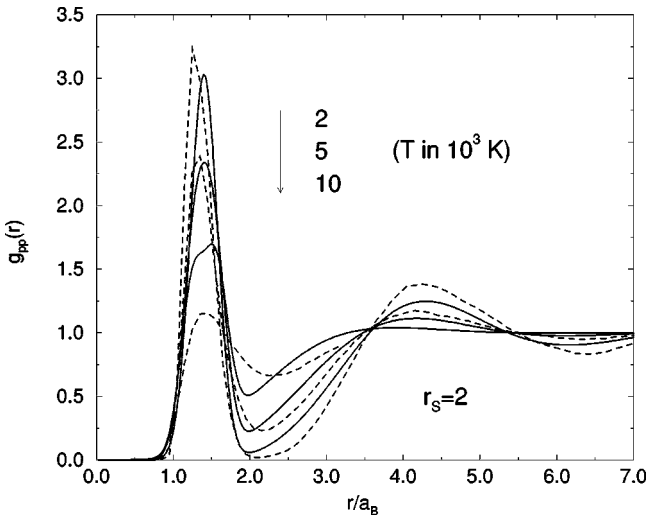

FIG. 5. Proton-proton pair distribution function for $r_s=2$ $\varrho=0.3344$ g/cm^3) and various temperatures: DM (solid lines) and TB-II (dashed lines).

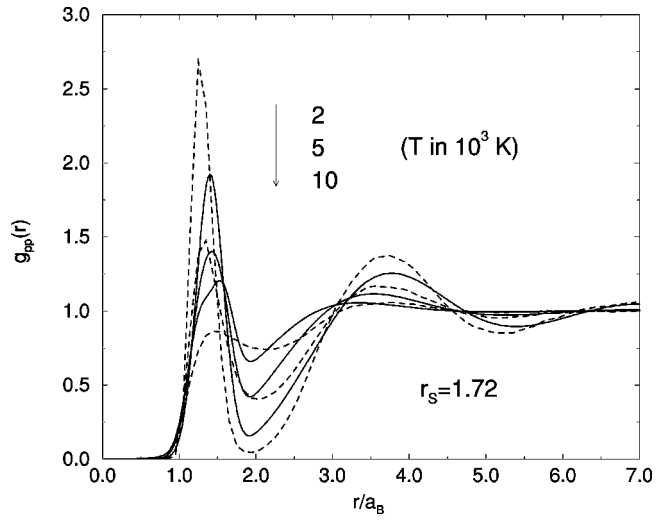

FIG. 6. As Fig. 5, but for $r_s=1.72$ ($\varrho=0.5257$ g/cm^3).

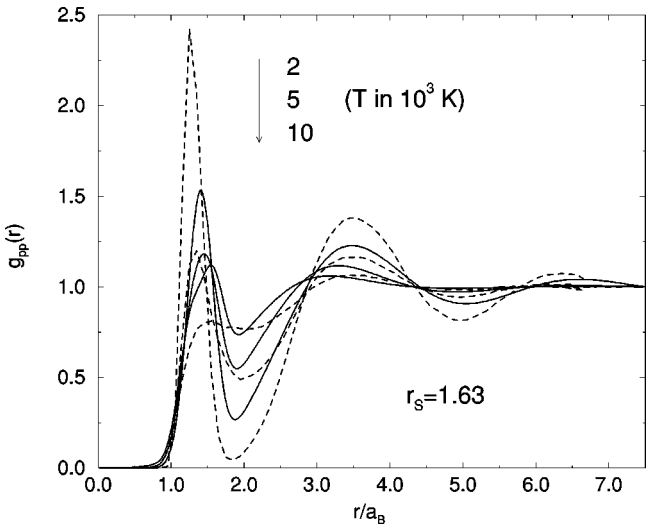

FIG. 7. As Fig. 5, but for $r_s=1.63$ ($\varrho=0.6177$ g/cm^3).

gives an average bond length or width of a distribution of molecular bonds found in the medium. For the TB case at 10 000 K, we must integrate to a radial value of almost $2a_B$ before obtaining a coordination number of 1, while this distance remains much smaller for the DM. Therefore, we obtain approximately the same β parameter, and by inference the same number of molecules, but with very different distributions of the bond lengths.

In Fig. 8, we next compare the Hugoniots [24] for the DM and TB with other theoretical formulations and with the NOVA laser and gas-gun experiments. Liquid molecular deuterium at cryogenic temperatures ($\rho_D=0.171$ g/cm^3, $T=20$ K) sets the initial conditions for the models and the laser and gas-gun shocks. The solid line denotes the results derived from the SESAME EOS [4], which represented a standard for H up to the advent of the laser experiments. The maximum compression reaches a value of about four, which appears similar to an ideal gas of atoms. The laser experiments [2,3] reach a maximum compression factor of 6, more in line with a rigid diatomic ideal gas, and remain considerably compressed even at rather high temperatures. SESAME and the model of Ross [25], both employ a minimization of the free energy to determine the EOS but emphasize different basic properties and techniques. The DM does not include ionization; its inclusion will demand an eventual return to the SESAME curve at higher pressures [26]. Both the TB and PIMC represent dynamical models and are in disagreement at low pressures. The TB-II follows the SESAME Hugoniot for most of its course, yielding only a slightly larger maximum compression (7%). TB-I, with a rather different set of fitting criteria, exhibits nearly the same behavior, while the PIMC shows a larger excursion. This trend to a higher compression in the PIMC seems closely tied to a phase transition that occurs around 10 000 K at deuterium densities of about 0.66 g/cm^3. Neither the TB nor the DF schemes (LDA or GGA) exhibit this phase transition under these conditions. The error bars in the laser experiments [2,3] range from about ± 0.1 g/cm^3 in the density at the lower pressures (<200 GPa) to about ± 0.2 g/cm^3 above this.

Comparing the TB and DM in more detail gives further insight into the behavior of various models in this regime. As indicated above, the two models contain the same basic physics that should govern the Hugoniot at least to maximum

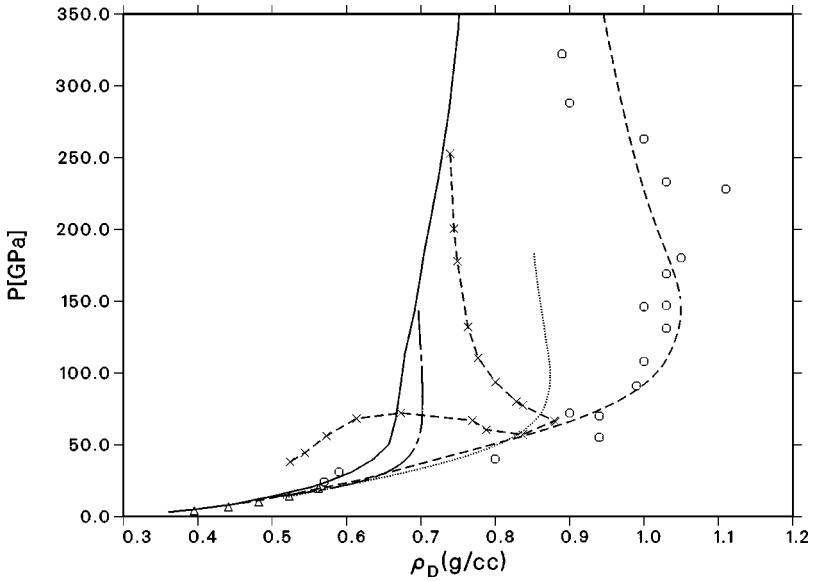

FIG. 8. Deuterium Hugoniots. Theoretical models: SESAME (line, Ref. [4]), TB-II (chain-dashed line), Ross (dashed line; Ref. [24]), DM (dotted line), and PIMC (crosses, Ref. [6]). Experiments: gas-gun (triangles, Ref. [1]) and laser (circles, Refs. [2,3]).

compression. TB contains ionization to some degree, which the DM does not; however, ionization does not appear as a major influence at these low temperatures [26]. The TB reaches about 15 000 K and the DM, about 20 000 K at maximum compression. Yet, the two models produce rather different predictions for the highest compression, the TB giving four and the DM, five. These differences do not appear to arise from any basic physical process found in one and not the other but must originate in sensitivites to the small differences in the two equations of state. As a comparison of these basic quantities demonstrate (Table I), these differences are subtle. The DM seems to reach higher compressions due to a somewhat later, slower release of the H_2 binding energy. An indication of this trend appears in the proton-proton PDF. Although the dissociation fraction between the TB and DM remain close in magnitude, the DM has more molecules in the lower vibrational states that yield more energy on dissociation.

IV. CONCLUSIONS

We have presented results for a TB model (TB-II) of hydrogen that considers more of the atomic and molecular characteristics, which are important in the neutral fluid domain at low temperatures, compared with a previous model (TB-I). We compare with corresponding results of a DM and the TB-I at some points in $\varrho - T$ space, which cover the region where a nonmetal-to-metal transition was observed recently.

A strong increase of the dissociation degree is obtained in both models when the medium heats and compresses. The agreement is reasonable considering the difficulties in defining this quantity in a consistent way in both models. Furthermore, the EOS data show good agreement for lower temperatures and densities. For hydrogen densities $\varrho \geqslant 0.5$ g/cm^3 and/or temperatures $T \geqslant 5000$ K where both models become increasingly uncertain, the discrepancies are more pronounced, especially for the pressure.

While the TBMD method includes, in principle, excited and ionized levels, the DM is restricted to a neutral H-H_2 mixture. The influence of ionization has been studied in [26] combining the present DM with known results for the EOS of fully ionized hydrogen plasma, see, e.g., [27,28]. The EOS of such a combined dissociation–ionization model for $T = (2-10) \times 10^3$ K and $\varrho_H \leqslant 2$ g/cm^3 shows a phase instability between 0.6 and 0.9 g/cm^3 which is connected with the hypothetical plasma phase transition. No indications of such a phase instability have been found in either the TB or DF models.

Besides the EOS data, we have compared also the resulting proton-proton PDFs extracted from the TBMD simulations and the DM. Again, the agreement is good at the lower temperatures $T \leqslant 7500$ K and densities $\varrho \leqslant 0.5$ g/cm^3, while systematic deviations occur in the remaining parameter region. However, the transition from a pure molecular liquid to a disordered monoatomic fluid at high densities and/or temperatures is clearly seen. The relation to the corresponding variation of the electronic properties, i.e., the nonmetal-to-metal transition as observed experimentally, has to be discussed by means of, e.g., the electrical conductivity. The TB and DF molecular-dynamics simulations all [29] display a distinct rise in conductivity at low temperature (< 5000 K) as a function of density in relatively good agreement with the gas-gun results [1]. This rise appears intimately associated with the degree of dissociation and, therefore, a similar trend is found in the DM when considering ionization in addition, see [30]. The conductivity reaches a plateau at a few thousand inverse ohm cm, corresponding to a liquid metal or semiconductor. The associated medium remains mainly molecular with some monomers and resembles more a conducting soup than a pure metal.

The Hugoniots show greater differences with the DM yielding a higher maximum compression. Since the models contain basically the same physical processes, these differences must arise from subtle sensitivities to the basic EOS data.

In this paper, we have compared several different models of hydrogen for low to intermediate densities and temperatures. While the techniques for generating these models differ considerably, they show rather good agreement through this regime. Therefore, the behavior of hydrogen under these conditions (dissociating fluid) is better and better understood. The region of ultrahigh densities and higher temperatures has to be probed further.

ACKNOWLEDGMENTS

This work was supported by the Deutsche Forschungsgemeinschaft within the Sonderforschungsbereich 198 Kinetics of Partially Ionized Plasmas. The work was also supported by the U.S. Department of Energy through Los Alamos National Laboratory.

[1] S. T. Weir, A. C. Mitchell, and W. J. Nellis, Phys. Rev. Lett. **76**, 1860 (1996).

[2] L. B. Da Silva, P. Celliers, G. W. Collins, K. S. Budil, N. C. Holmes, T. W. Barbee, Jr., B. A. Hammel, J. D. Kilkenny, R. J. Wallace, M. Ross, R. Cauble, A. Ng, and G. Chiu, Phys. Rev. Lett. **78**, 483 (1997).

[3] G. W. Collins, L. B. Da Silva, P. Celliers, D. M. Gould, M. E. Ford, R. J. Wallace, A. Ng, S. V. Weber, K. S. Budil, and R. Cauble, Science **281**, 1178 (1998).

[4] SESAME: The Los Alamos National Laboratory Equation of State Database Report No. LA-UR-92-3407, edited by S. P. Lyon and J. D. Johnson (unpublished); G. I. Kerley in *Molecular-Based Study of Fluids*, edited by J. M. Haile and G. A. Mansoori (American Chemical Society, Washington, DC, 1983), pp. 107–138.

[5] W. Ebeling, W.-D. Kraeft, and D. Kremp, *Theory of Bound States and Ionization Equilibrium in Plasmas and Solids* (Akademie-Verlag, Berlin, 1976).

[6] C. Pierleoni, D. M. Ceperley, B. Bernu, and W. R. Magro, Phys. Rev. Lett. **73**, 2145 (1994); W. R. Magro, D. M. Ceperley, C. Pierleoni, and B. Bernu, *ibid.* **76**, 1240 (1996).

[7] D. Klakow, C. Toepffer, and P.-G. Reinhard, Phys. Lett. A

192, 55 (1994); J. Chem. Phys. **101**, 10 766 (1994).
[8] L. Collins, I. Kwon, J. Kress, N. Troullier, and D. Lynch, Phys. Rev. E **52**, 6202 (1995).
[9] I. Kwon, L. Collins, J. Kress, and N. Troullier, Phys. Rev. E **54**, 2844 (1996).
[10] T. J. Lenosky, J. D. Kress, L. A. Collins, and I. Kwon, Phys. Rev. B **55**, R11 907 (1997); T. J. Lenosky, J. D. Kress, and L. A. Collins, *ibid.* **56**, 5164 (1997).
[11] A. Bunker, S. Nagel, R. Redmer, and G. Röpke, Phys. Rev. B **56**, 3094 (1997).
[12] A. Bunker, S. Nagel, R. Redmer, and G. Röpke, Contrib. Plasma Phys. **37**, 115 (1997); **37**, 469(E) (1997).
[13] S. Nagel, R. Redmer, G. Röpke, M. Knaup, and C. Toepffer, Phys. Rev. E **57**, 5572 (1998).
[14] I. Kwon, J. D. Kress, and L. A. Collins, Phys. Rev. B **50**, 9118 (1994).
[15] D. W. Schwenke, J. Chem. Phys. **89**, 2076 (1988).
[16] P. Loubeyre, R. Le Toullec, D. Hausermann, M. Hanfland, R. J. Hemley, H. K. Mao, and L. W. Finger, Nature (London) **383**, 702 (1996).
[17] G. Kresse and J. Hafner, Phys. Rev. B **47**, 558 (1993); **49**, 14 251 (1994); G. Kresse and J. Furthmüller, Comput. Mater. Sci. **6**, 15 (1996); Phys. Rev. B **54**, 11 169 (1996).
[18] K. P. Huber and G. Herzberg, *Molecular Spectra and Molecular Structure. Vol. IV: Constants of Diatomic Molecules* (Van Nostrand, New York, 1979).
[19] M. Ross, F. H. Ree, and D. A. Young, J. Chem. Phys. **79**, 1487 (1983).
[20] W. Kolos and L. Wolniewicz, J. Chem. Phys. **43**, 2429 (1965).
[21] F. Moshary, N. H. Chen, and I. F. Silvera, Phys. Rev. B **48**, 12 613 (1993).
[22] H. K. Mao and R. J. Hemley, Rev. Mod. Phys. **66**, 671 (1994).
[23] O. Pfaffenzeller and D. Hohl, J. Phys.: Condens. Matter **9**, 11 023 (1997).
[24] L. D. Landau and E. M. Lifshitz, *Fluid Mechanics* (Pergamon Press, Oxford, 1987).
[25] M. Ross, Phys. Rev. B **54**, R9589 (1996); **58**, 669 (1998).
[26] D. Beule, W. Ebeling, A. Förster, H. Juranek, R. Redmer, and G. Röpke, Contrib. Plasma Phys. **39**, 21 (1999); Phys. Rev. B **59**, 14 177 (1999).
[27] W. Ebeling and W. Richert, Phys. Status Solidi B **128**, 467 (1985); Phys. Lett. A **108**, 80 (1985); Contrib. Plasma Phys. **25**, 1 (1985).
[28] W. Ebeling, A. Förster, H. Hess, and M. Yu. Romanovsky, Plasma Phys. Controlled Fusion **38**, A31 (1996).
[29] T. Lenosky, J. Kress, L. Collins, and I. Kwon, J. Quant. Spectrosc. Radiat. Transf. **58**, 743 (1997).
[30] R. Redmer, G. Röpke, D. Beule, and W. Ebeling, Contrib. Plasma Phys. **39**, 25 (1999).